NURETH14-579

VALIDATION OF SUBCHANNEL CODE KAMUI: ANALYSIS OF OUTLET TEMPERATURE PROFILES OF A 19-PIN TEST ASSEMBLY

S. Pramuditya¹ and H. Ninokata¹

Tokyo Institute of Technology
N1-5, 2-12-1 Ookayama, Meguro-ku, Tokyo, Japan

Abstract

Thermal hydraulic analysis of a Sodium-cooled Fast Reactor test assembly has been performed by employing subchannel analysis code KAMUI. The code has been updated by incorporating some recent physical models for pressure drop and coolant mixing. Performance of several conventional flow resistance and mixing models was assessed, by comparing predicted outlet temperature profiles against available experimental data. The calculations were carried out for high, transitional, and low Reynolds number regions. The prediction capability of the code for a wire-wrapped bundle has been successfully demonstrated in this paper.

Introduction

The design of Sodium-cooled Fast Reactor (SFRs) cores requires an accurate thermal hydraulic prediction capability, this is generally related to the determination of maximum cladding and coolant temperatures which might exists in the reactor core. Thermal hydraulic analyses of a Sodium-cooled Fast Reactor (SFR) fuel subassembly can be performed in various levels of resolution. By the continuing development of computing power, it is now possible to carry out a 3D full bundle Computational Fluid Dynamics (CFD) calculation. However, these kind of high resolution calculations for a whole subassembly still require very large computational resources, and hence, are still not practical for general use. In this regard, subchannel analysis method can be considered more suitable for this task.

Subchannel analysis refers to coarse nodalization of the calculation domain (fuel assembly) into spatial meshes of a size equivalent to a single fluid volume between fuel rods. Several subchannel analysis codes, applicable for sodium coolant, have been developed in various countries for the past decades, these include KAMUI [1], SABENA [2], where both were designed for grid-spaced fuel pin subassemblies; ASFRE-III [3], COBRA-IV-I [4], SUPERENERGY II [5], and RELAP5-3D [6] for wire-wrapped pin subassemblies. The KAMUI code has been validated for sodium boiling experiment in many grid-spaced bundles. It was not designed for single phase flows in wire-wrapped pin subassemblies. Therefore, in this paper, the code is updated by incorporating recent models for flow resistance and intersubchannel mixing, and then validated against experimental data.

1. KAMUI Subchannel analysis code

KAMUI code was initially designed for Sodium-cooled Fast Reactor thermal hydraulics analysis under severe accident conditions. It is a multi-fluid multi-phase subchannel analysis code, which considers only a single subassembly. Two velocity fields are considered, one for sodium vapor, and the other for the mixture of liquid sodium, liquid steel, liquid fuel, and solid fuel particles. This work deals with single-phase sodium flows in a fuel assembly, and therefore, only single-phase governing equations and physical models will be described. The code simultaneously solves conservation equations of mass, energy, and momentum. Mass conservation equation is expressed as:

$$\frac{\partial \rho}{\partial t} + \nabla \cdot \left[\rho \vec{v} \right] = 0, \tag{1}$$

energy conservation equation is expressed as:

$$\frac{\partial}{\partial t} \left[\rho e \right] + \overrightarrow{\nabla} \cdot \left[\rho e \overrightarrow{v} \right] = q''' + k \nabla^2 T, \tag{2}$$

and momentum conservation equation is expressed as:

$$\frac{\partial}{\partial t} \left[\rho \vec{v} \right] + \vec{\nabla} \cdot \left[\rho \vec{v} \vec{v} \right] = -\nabla p + \rho g + \vec{\nabla} \cdot \vec{\tau}, \tag{3}$$

where $\rho, v, p, g, \tau, e, q$ ", k, and T are fluid density, fluid velocity, pressure, gravity acceleration, stress tensor, internal energy, volumetric heat generation rate, thermal conductivity, and temperature, respectively. The conservation equations are then discretized based on standard triangular subchannel geometry. Having all the conservation equations discretized, a Jacobian matrix is then constructed, the resulting non-linear equation system is numerically solved by multivariable Newton-Raphson method.

2. Physical model description

To solve the equation system briefly described in the previous section, we need to close the equation system by employing some constitutive equations, relating all the unknowns with the main variables (density, internal energy, and velocities). Since this paper deals only with single phase flow, only single phase flow models are described here. Two important mechanisms that need to be modeled by employing empirical correlations are flow resistance and inter-subchannel mixing.

2.1 Flow resistance models

There were three flow resistance models available in KAMUI code, in which the user specifies which model is to be used to carry out a calculation. The first one is simple flow resistance model for pipe, applicable for bare bundle calculations. This model consists of Darcy correlation for laminar flow, and the following correlation for turbulent flow:

$$f = 0.0055 \left[1 + \left(2000 \frac{\lambda}{D_e} + \frac{10^6}{\text{Re}} \right)^{1/3} \right], \tag{4}$$

where λ/D_e is defined as relative roughness of the surface. The transition Reynolds number of 1084 was chosen to avoid numerical instability caused by discontinuity of the flow resistance coefficient f.

The second one is flow resistance model to be used for wire-wrapped bundle calculations, which consists of Engel correlation for laminar flow [7]:

$$f = \frac{320}{\text{Re}\sqrt{H}} \left(\frac{P}{D}\right)^{1.5},\tag{5}$$

and Novendstern correlation for turbulent flow [8]:

$$f = 0.316 \,\mathrm{Re^{-0.25}} \times \left[\frac{1.034}{\left(P/D\right)^{0.124}} + \frac{29.7 \left(P/D\right)^{6.94} \,\mathrm{Re^{0.086}}}{\left(H/D\right)^{2.239}} \right]^{0.885}.$$
 (6)

And the third one is flow resistance model to be used for grid-spaced bundle calculations.

The Cheng-Todreas pressure drop model [9] has been incorporated into the code. This model takes into account the geometrical difference of each subchannel type (interior, edge, and corner). The correlation appears as polynomials for each subchannel type, for bare bundle, it is expressed as:

$$C_{fi}^* = a + b_1 \left[\frac{P}{D} - 1 \right] + b_2 \left[\frac{P}{D} - 1 \right]^2,$$
 (7)

where C_{fi}^* is bare bundle constant, and a, b_1 , and b_2 are some other empirical constants. For wire-wrapped bundle, two other empirical constants: wire drag and wire sweep constants, which depend on geometry and flow regime, must also be included. For wire-wrapped bundle, the correlations are expressed as:

$$C_{f1} = C_{f1}^* \left(\frac{P_{w1}^*}{P_{w1}}\right) + W_d \left(\frac{3A_{r1}}{A_1^*}\right) \left(\frac{D_{e1}}{H}\right) \left(\frac{D_{e1}}{D_w}\right)^m, \tag{8}$$

$$C_{f2} = C_{f2}^* \left[1 + W_s \left(\frac{A_{r2}}{A_2^*} \right) \tan^2 \theta \right]^{\frac{3-m}{2}}, \tag{9}$$

$$C_{f3} = C_{f3}^* \left[1 + W_s \left(\frac{A_{r3}}{A_3^*} \right) \tan^2 \theta \right]^{\frac{3-m}{2}}, \tag{10}$$

$$f_i = \frac{C_{fi}}{\text{Re}_{\cdot}^m},\tag{11}$$

where m=1 for laminar flow and m=0.18 for turbulent flow. And $C_{f,p}P_{wp}^*P_{wp}W_d,W_s,A_i^*,A_{rp}$ and θ are wire-wrapped bundle constant, wetted perimeter without wire, wetted perimeter including wire, drag coefficient, sweep coefficient, axial flow area without wire, wire projected area, and angle of the wire relative to axial direction, respectively. This pressure drop model is rather complicated, consisting of many geometrical parameters and empirical constants which depend on P/D ratio, subchannel type, and flow regime. A complete explanation can be found in [9]. It is well known that the Distributed Resistance Model (DRM) [10] accurately predicts the hydraulic resistance of wire-wrapped pin subassemblies, this model also will be incorporated into the code in the future.

2.2 Inter-subchannel mixing models

There are basically two mechanisms which create inter-subchannel mass exchange: diversion cross flow due to transverse pressure gradient, and mass interchange due to turbulent fluctuation in the axial flow. In wire-wrapped fuel bundle, the wire swirl also creates inter-subchannel mass exchange, due to its flow-sweeping effect. In KAMUI code, single phase turbulent mass interchange is assumed to involve equal mass of eddies crossing fluid-fluid boundaries.

Inter-subchannel momentum and energy exchange are created by three mechanisms: transport by diversion cross flow, transport by turbulent interchange, and transport by molecular/viscous effects. In KAMUI code, the inter-subchannel turbulent and molecular mixing of momentum and energy are modeled based on effective eddy diffusivity approach, they are considered in axial momentum and energy transport equations. Effective mixing flow rate is expressed as:

$$W_{ij}^* = \beta_i \, s_{ij} \overline{G}_k, \tag{12}$$

where \overline{G}_k is average axial mass flux of the interacting subchannels connected by gap k, and s_{ij} is gap width. W_{ij}^* includes both molecular and turbulent effects, and β_i is expressed as:

$$\beta_i = \frac{C_{mix}D_{V,k}}{\lambda_{ij} \operatorname{Re}_k^{0.125}},\tag{13}$$

where C_{mix} , $D_{V,k}$ and λ_{ij} are mixing coefficient, volumetric hydraulic diameter of the transverse momentum control volume at gap k, and effective mixing length, respectively. In

KAMUI, both laminar and turbulent mixing lengths are approximated as centroid distance of adjacent subchannels. Transverse momentum transport is expressed as:

$$F = W_{ij,M}^* \left[w_i - w_j \right], \tag{14}$$

and transverse energy transport is expressed as:

$$Q = W_{ij,H}^* C_p \left[T_i - T_j \right], \tag{15}$$

where C_p is specific heat capacity, and T is coolant temperature. It is well-known that the effective cross flow for transverse energy transport, $W_{ij,H}^*$, and for momentum transport, $W_{ij,M}^*$, are not necessarily identical, in KAMUI however, it is assumed that they simply equal to W_{ij}^* . The Cheng-Todreas mixing model [9] has been implemented into the code. This model evaluates effective mixing flow rate differently for interior and peripheral zones. For interior zone, mixing flow rate is expressed as:

$$W_{ii}^* = \rho_i \, \varepsilon^* v_i \, s_{ii}, \tag{16}$$

where ρ_i and v_i are fluid density, axial velocity in interior subchannel *i* respectively. The dimensionless eddy diffusivity for turbulent flows is calculated as follow:

$$\varepsilon^* = 0.14 \left(\frac{s_{ij}}{D}\right)^{-0.5} \left(\frac{A_{r1}}{A_1'}\right)^{0.5} \tan \theta,\tag{17}$$

where A_{r1} and A'_{l} are wire projected area and bare rod flow area of interior subchannels, respectively. And $\tan \theta$ is defined as follows:

$$\tan \theta = \frac{\pi \left(D + D_w \right)}{H}.$$
 (18)

In peripheral subchannels, a coherent swirl flow transporting both momentum and energy exists. The effect of this swirl flow to the transport of heat is also modeled by the effective mixing flow rate. This flow rate for peripheral subchannels is expressed as:

$$W_{ii}^* = \rho_i C_{IL} v_i s_{ii}, \tag{19}$$

where C_{IL} is the ratio of lateral to axial velocities, and for turbulent flows, it is expressed as:

$$C_{IL} = 0.75 \left(\frac{H}{D}\right)^{0.3} \left(\frac{A_{r2}}{A_2'}\right)^{0.5} \tan\theta,$$
 (20)

where $A_{r,2}$ and A'_{2} are wire projected area and bare rod flow area of edge subchannels, respectively.

3. Analysis of ORNL 19-pin experimental data

The capability and accuracy of the KAMUI code, as well as the performance of the physical models described in the previous section will be evaluated. The evaluation was carried out by performing calculations based on available experimental data taken from ref. [11], the effects of the models on the calculation results will be described. This also serves as an effort to validate the KAMUI code, that is to asses the proper coding of the code and its prediction capability for single-phase flows wire-wrapped bundle calculations. The test assembly contains 19 electrically heated rods within a hexagonal wrapper can, which has pitch to pin diameter (P/D) ratio of 1.243 and wire wrap axial pitch to pin diameter ratio (H/D) of 52.2. A summary of the test bundle characteristics is shown in Table 1.

Parameters	Value	
Fluid	Sodium	
Number of rods	19	
Simulated length [mm]	914.4 (36 in.)	
Heated length [mm]	533.4 (21 in.)	
Rod diameter (D) [mm]	5.842 (0.230 in.)	
Interior pitch (P) [mm]	7.2644 (0.286 in.)	
P/D	1.243	
Edge pitch (W) [mm]	7.3914 (0.291 in.)	
W/D	1.265	
Wire diameter [mm]	1.4224 (0.056 in.)	
Wire axial pitch (H) [mm]	304.8 (12 in.)	
H/D	52.2	
Flat to flat distance [mm]	34.1 (1.343 in.)	
Axial power profile	Uniform	
System pressure [Pa]	1.0132E+5	
Inlet temperature [K]	588.5 (600 F)	

Sodium outlet temperatures were measured by exit thermocouple rake, located 76.2 mm (3 in.) from the top of heated section. The total length to be simulated in this work is 914.4 mm (36 in.), consisting of 304.8 mm (12 in.) unheated zone at the bottom, 533.4 mm (21 in.) heated zone, and 76.2 mm (3 in.) unheated zone on the top.

To perform the calculations, the test bundle is axially divided into 36 and/or 72 cells, plus one fictitious cell at the bottom and another one on the top, used to impose boundary conditions. Therefore, the calculational domain consists of 38 and/or 74 axial planes, and 42 subchannels, equals to 1596 and/or 3108 fluid cells in total. The choice of the number of axial cells (38 or 74) will be explained later. Pin, subchannel, and gap numbering schemes are shown as follow:

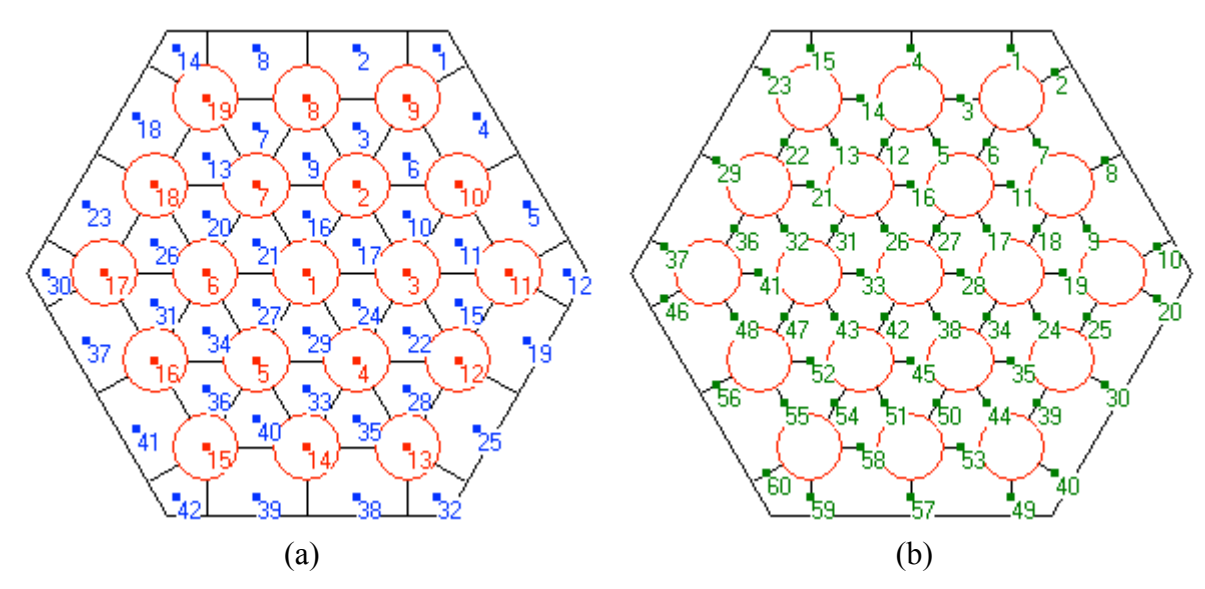


Figure 1 Numbering schemes: (a) pin and subchannel; (b) gap

Subchannel analysis is a lumped parameter method, which employs a relatively large spatial mesh, therefore, accurate modeling plays an important role to produce results that match experimental data. When performing numerical simulation, thermal hydraulic characteristics of wire-wrapped bundles are mostly affected by two parameters: flow resistance model, and mixing model.

Several calculations for the same case were carried out by employing different models for flow resistance and inter-subchannel mixing, aimed at comparing the performance of each model. The selected experimental data for these calculations was the high flow-high power case of the experiment [11], that is run number 022472, with volumetric flow rate of 3.47E-3 m^3/s , and bundle total power of 322525 W. The calculation matrix is shown as follow:

Case name	Flow resistance model	Mixing model
Case1	Novendstern	Eq. (12)
Case2	Cheng-Todreas	Cheng-Todreas

The actual boundary condition needed to run the calculation is total mass flow rate, equals to volumetric flow rate multiplied by reference density. Kim et al. [12] performed subchannel analysis for the same case, he used the value of 3.038 kg/s as the total mass flow rate, whereas Memmott et al. [6] used 3.08 kg/s on his paper. The calculation results by using these two values of total mass flow rate will be described later. First of all, to assure that the results are grid-independent, two calculations have been performed by using different axial mesh size, one is 2.54 cm (38 axial meshes), and the other is 1.27 cm (74 axial meshes).

Table 3. Effect of axial mesh size on calculation results

The 14th International Topical Meeting on Nuclear Reactor Thermalhydraulics, NURETH-14 Toronto, Ontario, Canada, September 25-30, 2011

	ρ [kg/m3]	T[K]	w [m/s]
Maximum (38 / 74meshes)	876.37 / 876.37	713.16 / 713.30	8.36 / 7.60
Average (38 /74 meshes)	865.98 / 865.97	630.91 / 630.91	8.36 / 7.60

Table 3 compares the calculation results by employing different mesh number, we can see that the results are essentially the same, thus, justifying the use of 38 axial meshes, which is preferable when one considers calculational running time. Therefore all the following calculations were carried out by using 38 axial meshes.

Comparison with experimental data is made in terms of normalized outlet temperature, which is defined as:

$$T^* = \frac{T_i - T_{in}}{T_{out,avg} - T_{in}},$$
(21)

where T_i , T_{in} , and $T_{out,avg}$ are temperature of subchannel i, inlet temperature, and average outlet temperature, respectively. While some researcher [13] perform the temperature averaging process only over flow area, here the outlet temperature is averaged over mass flow rate at each subchannel, since this is physically more appropriate. Average outlet temperature is then expressed as:

$$T_{out,avg} = \frac{\sum_{i=1}^{N} T_{i} \ \rho_{i} \ w_{i} \ A_{i}}{\sum_{i=1}^{N} \rho_{i} \ w_{i} \ A_{i}},$$
(22)

where ρ_i , w_i , and A_i are density, axial velocity, and flow area of subchannel i, respectively. Note that since mass and energy cells (associated with T and ρ variables) are axially staggered by half mesh relative to axial momentum cells, the axial velocity variable in Eq. (22) is taken as an average value of two adjacent axial momentum cells.

Figure 2 compares calculation results for Case 1 and Case 2 (see Table 2), and by using total mass flow rate of 3.08 kg/s and 3.038 kg/s. We can see that the results obtained by employing the two mass flow rates are very similar. From visual inspection, we can also see that Case 2 (employing Cheng-Todreas flow resistance and mixing models) agrees better with the experimental data, compare to Case 1 (employing Novendstern flow resistance model, and mixing model expressed by Eq. (12)). The maximum error of Case 2 is ~14.7%, while its *Root Mean Square* (RMS) error is ~9.3%.

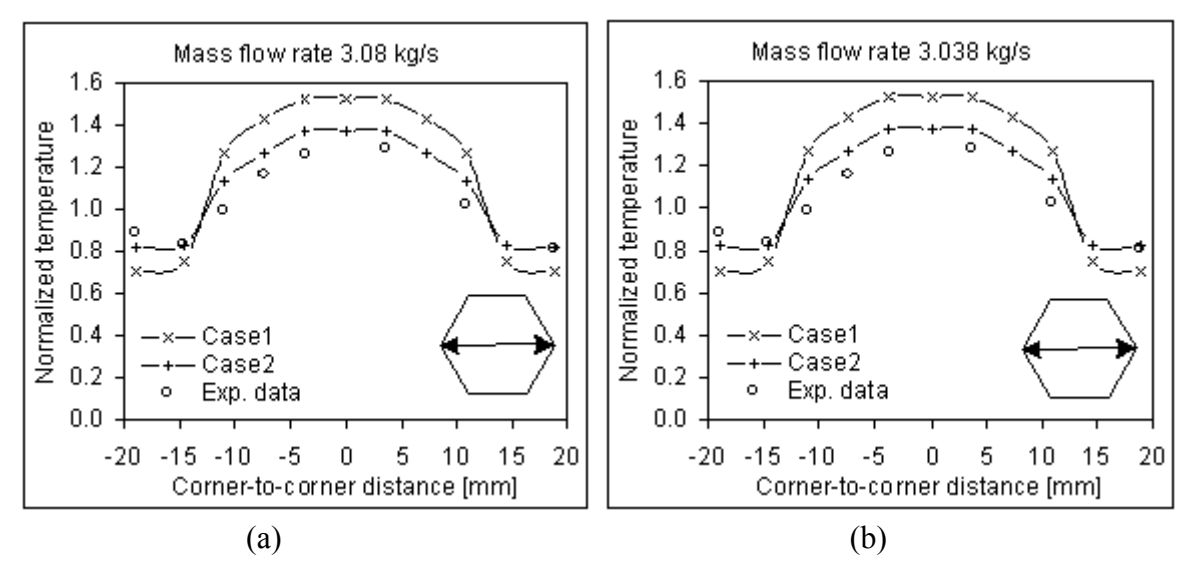


Figure 2 Comparison of predicted outlet temperature profile and experimental data: (a) mass flow rate 3.08 kg/s; (b) mass flow rate 3.038 kg/s

However, it was found that the average outlet temperature differs by about 6 K lower than the experimental data. This is possibly because the reference density used to determine the mass flow rate is not really correct. The mass flow rate can be calculated by either multiplying volumetric flow rate by density at inlet temperature, or by applying energy balance equation for the bundle. By using energy balance equation, to obtain a correct average outlet temperature of 676.3 K, the mass flow rate should be 2.86 kg/s, although it was found that the outlet temperature profile does not change so much when this value is used as boundary condition. Coolant outlet temperatures at peripheral subchannels are lower mainly because flow area in peripheral region is larger than the interior region. All the calculations previously described were carried out by using cold (nominal) dimension of the bundle. In reality, both the fuel pin and wire spacer experience thermal expansion, such that the ratio of peripheral to interior region flow area will be reduced. That is we assume that in actual operating conditions, the rod bundle comes in contact with the duct wall due to thermal expansion.

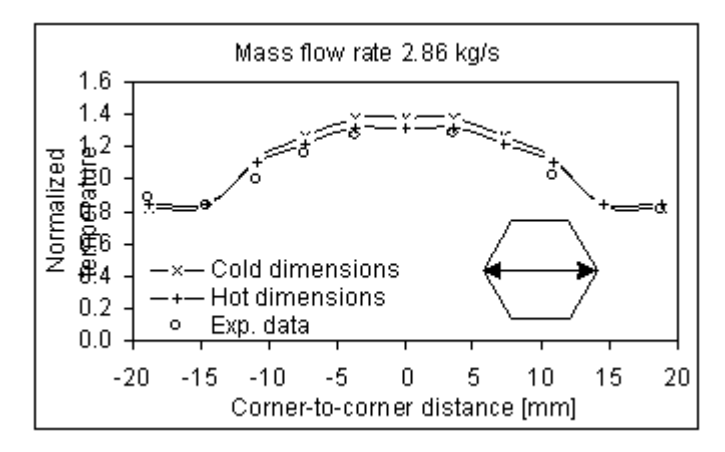


Figure 3 Comparison of predicted outlet temperature profile and experimental data by employing cold and hot dimensions

Figure 3 shows the calculation result when thermal expansion of fuel bundle is taken into account (hot dimension). What we mean with the term hot dimensions here is we assume that the physical size of both the pin and the wire spacer becomes slightly larger due to thermal expansion phenomena, such that the gap width is equal to wire diameter, and therefore, the bundle comes into contact with the duct wall. It was found that this condition is met when it is assumed that pin and wire diameters are expanded by 0.75% of their nominal (cold dimension) values.

By using hot dimension of the bundle, it was found that the calculated outlet temperature profile becomes flatter, and the maximum and RMS errors for this case are 11.9% and 6.2%, respectively. To further assess the prediction capability of the code, other calculations for run numbers with lower Reynolds number have also been performed. The first one is run number 020372, with bundle total power of 31255 W, and mass flow rate of 2.2927E-1 kg/s. And the second one is run number 020472, with bundle total power of 4987.5 W, and mass flow rate of 3.5980E-2 kg/s. The calculations were carried out by employing Cheng-Todreas flow resistance and mixing models, and using hot dimensions of the bundle.

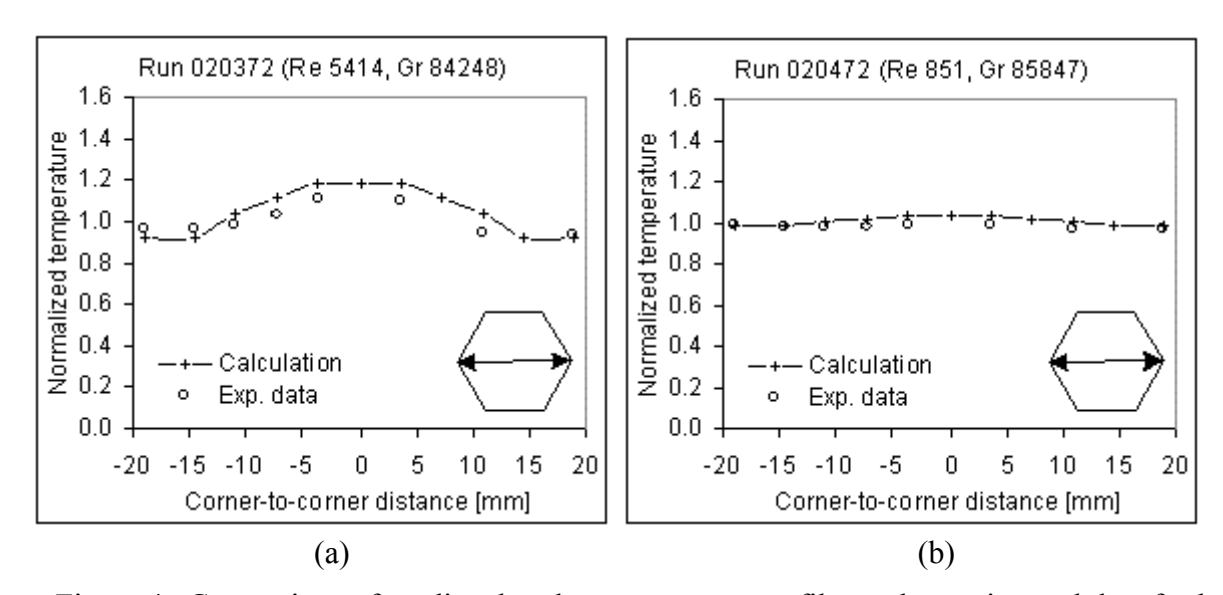


Figure 4 Comparison of predicted outlet temperature profiles and experimental data for low Reynold number cases

Figure 4a compares the predicted temperature profile and the experimental data for transitional Reynolds number of about 5000. As we can see that the agreement is acceptable, in which the maximum and RMS errors for this case are 10.2% and 6.9%, respectively. Figure 4b shows the calculation result for low Reynolds number of about 850. At low flow conditions, the effects of coolant conduction become important, in particular because sodium coolant has a high thermal conductivity. Conduction in lateral direction tends to flatten the temperature profile, as clearly shown by the experimental data. The agreement between calculation result and experimental data for this low flow case is relatively good, in which the maximum and RMS errors are 5.2% and 3.5%, respectively.

4. Conclusion

As a lumped parameter method, the accuracy of subchannel analysis depends on the performance of various physical models employed to perform the calculations. Two important parameters which significantly affect the calculation results are flow resistance model and inter-subchannel mixing model. The KAMUI code has now been updated by incorporating more recent flow resistance and mixing models. The prediction capability of the KAMUI code for single phase flows in a wire-wrapped bundle has been successfully demonstrated, in which simulations for the three run numbers have acceptable maximum and RMS errors between 5.2-11.9%, and 3.5-6.9%, respectively.

5. References

- [1] Kasahara, F., Ninokata, H., "The multi-fluid multi-phase subchannel analysis code KAMUI for subassembly accident analysis of an LMFR", *Journal of Nuclear Science and Technology*, Vol. 37, No. 8, 2000, pp. 654-669.
- [2] Ninokata, H., and Okano, T., "SABENA: subassembly boiling evolution numerical analysis", *Nuclear Engineering and Design*, Vol. 120, No. 2-3, 1990, pp. 349-367.
- [3] Ninokata, H., Deguchi, A., Baba, K., "ASFRE-III: A Computer Program for Triangular Rod Array Thermohydraulic Analysis of Fast Breeder Reactors", *PNC N941 85-106*, Oarai Engineering Center, Power Reactor and Nuclear Fuel Development Corporation, 1985.
- [4] Wheeler, C.L., "COBRA-IV-I: an interim version of COBRA for thermal-hydraulic analysis of rod bundles nuclear fuel elements and cores", *BNWL-1962*, 1976.
- [5] Basehore, K.L., Todreas, N.E., "SUPERENERGY-2: a multiassembly steady-state computer code for LMFBR core thermal-hydraulic analysis", *PNL-3379*, Pacific Northwest Laboratory, Richland, WA, 1980.
- [6] Memmott, M., Buongiorno, J., Hejzlar, P., "On the use of RELAP5-3D as a subchannel analysis code", *Nuclear Engineering and Design*, Vol. 240, No. 4, 2010, pp. 807-815.
- [7] Engel, F. C., Markley, R.A., and Bishop, A.A., "Laminar, transition and turbulent parallel flow pressure drop across wire-wrap-spaced rod bundle", *Nuclear Science and Engineering*, Vol. 69, 1979, pp. 290-296.
- [8] Novendstern, E.H., "Turbulent flow pressure drop model for fuel rod assemblies utilizing a helical wire-wrap spacer system", *Nuclear Engineering and Design*, Vol. 22, No. 1, 1972, pp. 28-42.
- [9] Cheng, S-K., Todreas, N. E., "Hydrodynamic models and correlations for bare and wire-wrapped hexagonal rod bundles -- Bundle friction factors, subchannel friction factors and mixing parameters", *Nuclear Engineering and Design*, Vol. 92, No. 2, 1986, pp. 227-251.

- [10] Ninokata, H., Efthimiadis, A., Todreas, N.E., "Distributed resistance modeling of wirewrapped rod bundles", *Nuclear Engineering and Design*, Vol. 104, No. 1, 1987, pp. 93-102.
- [11] M.H. Fontana, R.E. MacPherson, P.A. Gnadt and L.F. Parsly, "Temperature distribution in the duct wall and at the exit of a 19-rod simulated LMFBR fuel assembly (FFM Bundle 2A)", *Nuclear Technology*, Vol. 24, 1974, pp. 176–200.
- [12] Won-Seok Kim, Young-Gyun Kim, Young-Jin Kim, "A subchannel analysis code MATRA-LMR for wire wrapped LMR subassembly", *Annals of Nuclear Energy*, Vol. 29, No. 3, 2002, Pages 303-321.
- [13] Kamide, H., Hayashi, K., Toda, S., "An experimental study of inter-subassembly heat transfer during natural circulation decay heat removal in fast breeder reactors", *Nuclear Engineering and Design*, Vol. 183, No. 1-2, 1998, pp. 97-106.